Silicon nanowire array/Cu_2O crystalline core–shell nanosystem for solar-driven photocatalytic water splitting

2013 Nanotechnology 24 265402

(http://iopscience.iop.org/0957-4484/24/26/265402)

Nanotechnology **24** (2013) 265402 (8pp) doi:10.1088/0957-4484/24/26/265402

Silicon nanowire array/Cu_2O crystalline core–shell nanosystem for solar-driven photocatalytic water splitting

Zuzhou Xiong[1], Maojun Zheng[1], Sida Liu[1], Li Ma[2] and Wenzhong Shen[1]

[1] Key Laboratory of Artificial Structures and Quantum Control (Ministry of Education), Department of Physics, Shanghai Jiao Tong University, Shanghai, 200240, People's Republic of China
[2] School of Chemistry and Chemical Technology, Shanghai Jiao Tong University, Shanghai, 200240, People's Republic of China

E-mail: mjzheng@sjtu.edu.cn

Received 20 March 2013, in final form 16 May 2013
Published 3 June 2013
Online at stacks.iop.org/Nano/24/265402

Abstract

P-type Cu_2O nanocrystals were deposited on n-type silicon nanowire arrays (Si NWs) to form core–shell heterojunction arrays structure via a simple electroless deposition technique. Scanning electron microscopy, transmission electron microscope and x-ray diffraction were utilized to characterize the morphology and structure of the core–shell nanosystem. The reflectivity of the obtained core–shell structure measured by UV/vis spectrometry showed a comparatively low reflectivity in the visible-light region, which implied good optical absorption performance. The water splitting performance of the obtained Si NWs, planar Si/Cu_2O structure and Si NW/Cu_2O core–shell nanosystem were studied. Owing to the large specific surface area, heterojunctions formed between Cu_2O nanocrystallites and Si NWs and the light trapping effect of the NW array structure, the photocatalytic performance of the Si NW/Cu_2O core–shell nanosystem increased markedly compared with that of pure silicon NWs and a planar Si/Cu_2O structure, which means excellent hydrogen production capacity under irradiation with simulated sunlight. In addition, the photocatalytic performance of the core–shell nanosystem was improved obviously after platinum nanoparticles were electrodeposited on it.

(Some figures may appear in colour only in the online journal)

1. Introduction

Direct splitting of water using a semiconductor material under solar irradiation to produce clean and recyclable hydrogen on a large scale would be one of the best ways to solve the problems of energy shortages and environmental pollution. Since the pioneering work of Fujishima and Honda in 1972 [1], tremendous research on semiconductor-based photocatalysis and photoelectrolysis has yielded a better understanding of the mechanisms involved in photocatalytic and photoelectrochemical splitting of water [2–5]. Although a large number of semiconductor materials have been developed as good candidates for photoelectrodes and photocatalysts in past decades, the solar–hydrogen conversion efficiencies of these recognized materials are still not high enough. A nanostructured semiconductor photoelectrode or photocatalyst, which absorbs solar light more effectively and where solar-driven catalytic reactions take place, would play a critical role in the process of solar-driven water splitting. Thus, the design of efficient solar-active nanostructured materials has been the topic of considerable research [6–9].

Silicon is an attractive semiconductor material for constructing photoelectrodes or photocatalysts because of its abundance and unique electronic structure characteristics [10]. The study of silicon and its composite structure for use as a photocathode and photocatalyst in solar-driven water splitting has been going on for a long time [11–14]. Nanostructured silicon [15, 16], especially silicon nanowires

(NWs) [17–20], and its composite heterojunction [21–25] used as a photoelectrode and photocatalyst has attracted more and more interest in recent years, and nanostructured silicon has been regarded as a very promising material for generating hydrogen from splitting water. In addition, as an inexpensive and eco-friendly material, Cu_2O exists as a cuprite abundantly in nature, and has also been investigated extensively since Cu_2O is a simple metal oxide semiconductor with small band gap energy of 2.0–2.2 eV [26, 27]. To date, it has been widely utilized as an active component in electrode materials, solar cells, superconductors and so on. The conduction and valence band edges of Cu_2O seem to be available for reduction and oxidation of water, respectively, while the low band gap of Cu_2O means that it can absorb visible light effectively. So it is considered as an ideal photocatalytic material for hydrogen generation. Nanostructured Cu_2O [28–35] and its composite structure [36–41] used in photocatalytic water splitting have been investigated extensively, both theoretically and in experiments, in the past decade.

In this paper we report a Si NW/Cu_2O nanocrystal core–shell heterojunction structure nanosystem photocatalyst by a simple electroless deposition technique. This structure enhances charge separation and transport of photo-induced carriers due to the heterojunction, and impels carriers to travel to the electrolyte/catalyst interface. Furthermore, the Cu_2O nanocrystalline layer with a large surface area can improve the overall effective area for the photochemical reaction, thus improving the photocatalytic activity. The results demonstrate that the nanostructure heterojunction is of great importance for optimizing the photocatalytic performance of generation of hydrogen from water splitting. We also investigated the photocatalytic activity of the core–shell nanosystem with a platinum loading.

2. Experimental procedures

2.1. Silicon NW array fabrication

Highly oriented Si NW arrays on the silicon wafers were fabricated by a metal-assisted chemical etching method at room temperature.

(1) N-type Si wafers (1.5 cm × 1.5 cm, 380 μm thick, 10–20 Ω cm resistivity) were cleaned by soaking in acetone for 30 min and then by ultrasonic cleaning for 5 min. After being rinsed with de-ionized water, they were soaked in ethanol for 10 min then rinsed with de-ionized water again. Then they were dipped into H_2SO_4/H_2O_2[H_2SO_4(97%)/H_2O_2(30%) = 3:1] for 30 min. After rinsing with de-ionized water thoroughly, the Si wafer was immersed in HF solution for 1 min to wipe off the silica layer of the surface.

(2) Ag nanoparticles were deposited on the Si wafer by putting it into a mixed solution of 5 M HF and 0.005 M $AgNO_3$ for 90 s.

(3) Si NW arrays were obtained finally after putting the Si wafers covered with Ag nanoparticles into HF-based aqueous chemical etching solutions (composed of 4.6 M HF and 0.4 M H_2O_2) for 60 min.

2.2. Fabrication of the Si NW/Cu_2O nanocrystal and planar Si/Cu_2O composite structure

Si NW/Cu_2O nanocrystal core–shell structure and planar Si/Cu_2O structures were obtained via an electroless deposition technique. Fifty milliliters of 0.2 M $C_4H_4O_6NaK_4H_2O$ was added to 100 ml 0.15 M $CuSO_4$ solution under constant stirring. Ten minutes later, 5 ml of 1 M HCHO solution was added to the mixed solution drop by drop. Next, 2 M of NaOH solution was added slowly to regulate the pH value to about 13, then the mixed solution was put into a thermostatic water bath and heated to 45 °C. After leaving the Si NWs and Si wafers in the solution for different times, they were taken out and washed with ultrapure water.

2.3. Deposition of platinum nanoparticles

Platinum nanoparticles served as a co-catalyst and were potentiostatically electrodeposited in 200 ml of 1 mM H_2PtCl_6 solution at −0.1 V versus a standard Ag/AgCl reference electrode at room temperature. The deposition times were 10 min and 20 min respectively.

2.4. Surface morphology, structural characterization

The surface morphology of the Si NWs and Si NWs/Cu_2O samples was characterized by field emission scanning electron microscopy (FE-SEM; Philips Sirion 200, Philips, Netherlands) equipped with an energy dispersive x-ray spectrometer (EDS) system, and Pt nanoparticles were characterized by transmission electron microscopy (TEM; JEM-2100F, JEOL Ltd, Japan). The structure of the core–shell nanosystem was characterized by x-ray diffraction (XRD; D8 DISCOVER x-ray diffractometer, Bruker, Germany) with Cu Kα radiation (λ = 1.5406 Å).

2.5. Measurement of reflectance spectrum and photocatalytic performance

Reflectance spectra of the obtained Si NWs, planar Si/Cu_2O structure and Si NWs/Cu_2O core–shell nanosystem were collected using a UV/vis spectrometer (Lambda 20, Perkin Elmer, Inc., USA). The photocatalytic performance of Si NWs, planar Si/Cu_2O structure, Si NW/Cu_2O core–shell nanosystem, Pt-loaded Si NWs and Pt-loaded Si NW/Cu_2O core–shell nanosystem was investigated in a gas-closed circulation system (Labsolar-III Beijing Perfectlight Technology Co. Ltd, China) with a top window Pyrex cell. A 300 W Xe lamp (SOLAREDGE700, Beijing Perfectlight Technology Co. Ltd, China) was used as the light source; the luminous power of the light source was about 40 W. The amount of H_2 evolved was analyzed by an online gas chromatograph (GC7900, Techcomp LTD., China) equipped with a thermal conductivity detector (TCD) and MS-5A column; N_2 was used as the carrier. In all experiments, 100 ml of de-ionized water containing the mixed sacrificial agent, composed of 0.25 M Na_2SO_3 and 0.35 M Na_2S, was added to the reaction cell, which eliminated the photogenerated

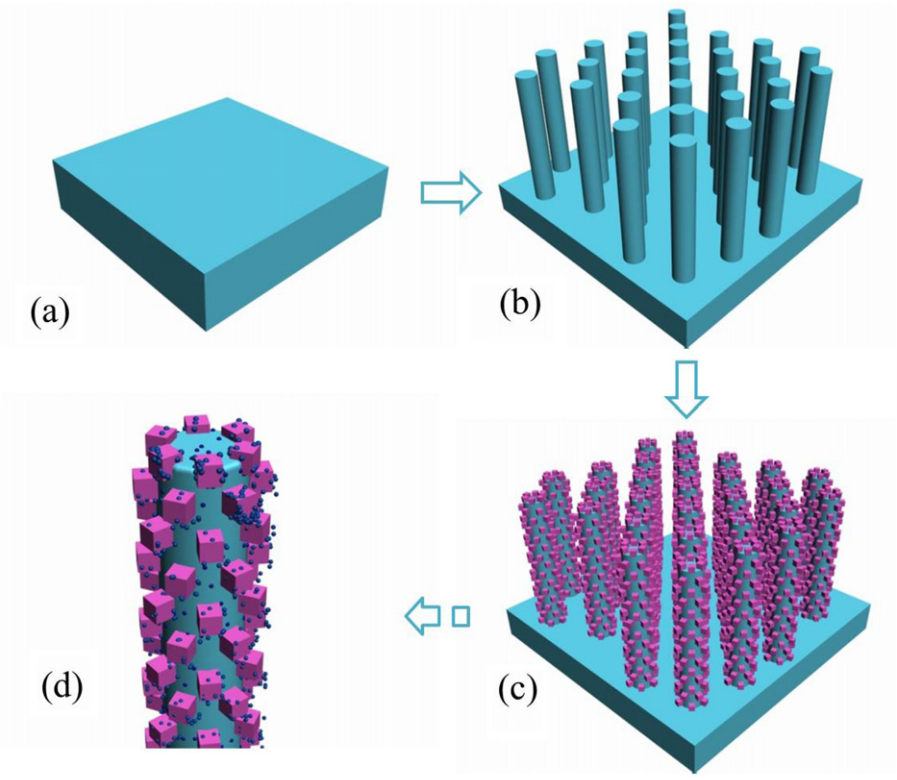

Figure 1. Schematic diagram of the fabrication process for the Si NW/Cu_2O core–shell nanosystem: (a) Si wafer, (b) Si NWs fabricated via metal-assisted chemical etching, (c) Cu_2O nanocrystallites deposited on Si NWs via electroless deposition, and (d) Si NW/Cu_2O core–shell nanosystem with Pt loading.

holes. Then these photocatalysts were put directly into the electrolyte solution. The whole system was pumped out with a vacuum pump before reaction to remove the dissolved air. The temperature for all photocatalytic reactions was kept at about 25 °C.

3. Results and discussions

Figure 1 shows a schematic diagram of the fabrication process of the core–shell nanosystem. After the silica layer was removed, a silicon wafer was put into the mixed solution consisting of 5 M HF and 0.005 M $AgNO_3$, in which a galvanic displacement reaction occurred [43]. That is, the reduction of metal ions (cathodic process) and the oxidation of Si atoms (anodic process) occurred simultaneously at the Si surface, while the charge is exchanged through the Si substrate:

$$Ag^+ + e^-_{VB} \rightarrow Ag^0(s) \quad (1)$$

$$Si(s) + 2H_2O \rightarrow SiO_2 + 4H^+ + 4e^-_{VB} \quad (2)$$

$$SiO_2(s) + 6HF \rightarrow H_2SiF_6 + 2H_2. \quad (3)$$

Then a thin silver nanoparticle film appeared on the surface of the silicon wafer. The formation of Si NW arrays can be explained basically by a Ag nanoparticle-catalyzed chemical etching model [42, 43]. The silicon underneath the Ag clusters acts as the anode, which is locally oxidized into SiO_2, and the dissolution of SiO_2 by HF results in the immediate formation of shallow pits under the Ag clusters. Ag clusters act as cathodes that serve to transport the electrons released from Si to facilitate Si oxidation, and are successfully preserved to gradually sink downwards into etched pits.

The mechanism of electroless deposition of Cu_2O nanocrystals on Si NW arrays can be depicted as follows [44]. Formaldehyde worked as the reduction agent, and when the pH value of the solution is up to about 13 the number of OH^- ions is large enough for the following chemical reaction to occur:

$$2Cu^+ + H_2O + 2OH^- \rightarrow Cu_2O + 2H_2O. \quad (4)$$

The surface morphology of Si NW arrays and Si NW/Cu_2O core–shell nanostructures is shown in figures 2 and 3. Figures 2(a) and (b) are top and cross-sectional views of the Si NW arrays. The diameter and the length of the Si NW are about 80–200 nm and 10 μm, respectively. Figures 2(c), (d) and 3 are top and cross-sectional views of the Si/Cu_2O core–shell NW arrays with different deposition times of Cu_2O nanocrystallite. They distributed on the surface of Si NW uniformly, and formed a perfect core–shell structure. When the deposition time was 2 min, there existed a thin Cu_2O nanocrystalline layer on the surface of the Si NWs (figures 2(c) and (d)). When the deposition time increased to 15 min, these Cu_2O nanocrystallites appeared as cubes, and the surface area of the core–shell structure was augmented markedly (figures 3(c) and (d)).

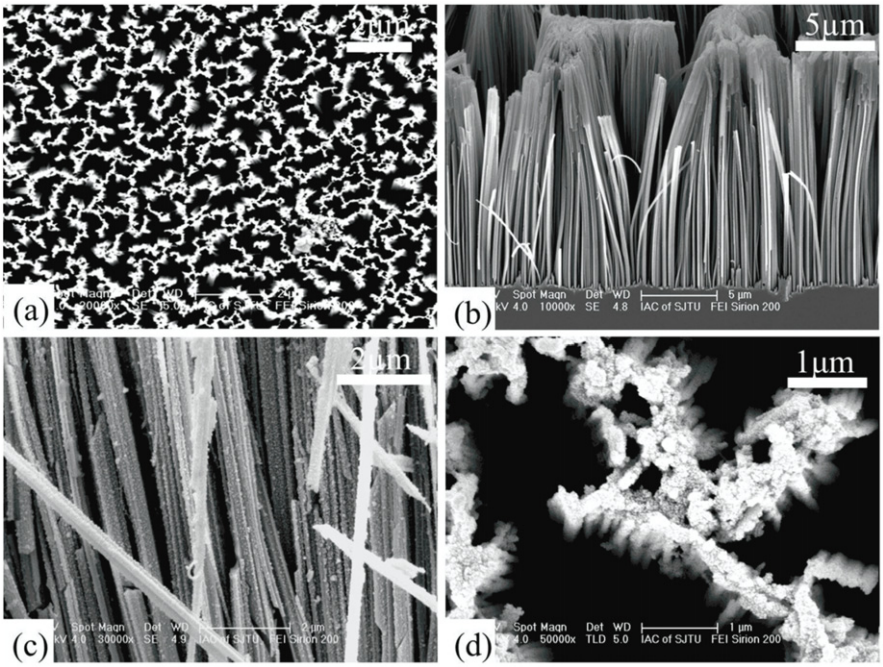

Figure 2. SEM images of Si NWs and Si NW/Cu_2O core–shell nanostructure: (a) top-view and (b) cross-sectional view of Si NWs, (c) cross-sectional view and (d) top-view of Si NW/Cu_2O core–shell nanostructure with 2 min deposition of Cu_2O nanocrystallite.

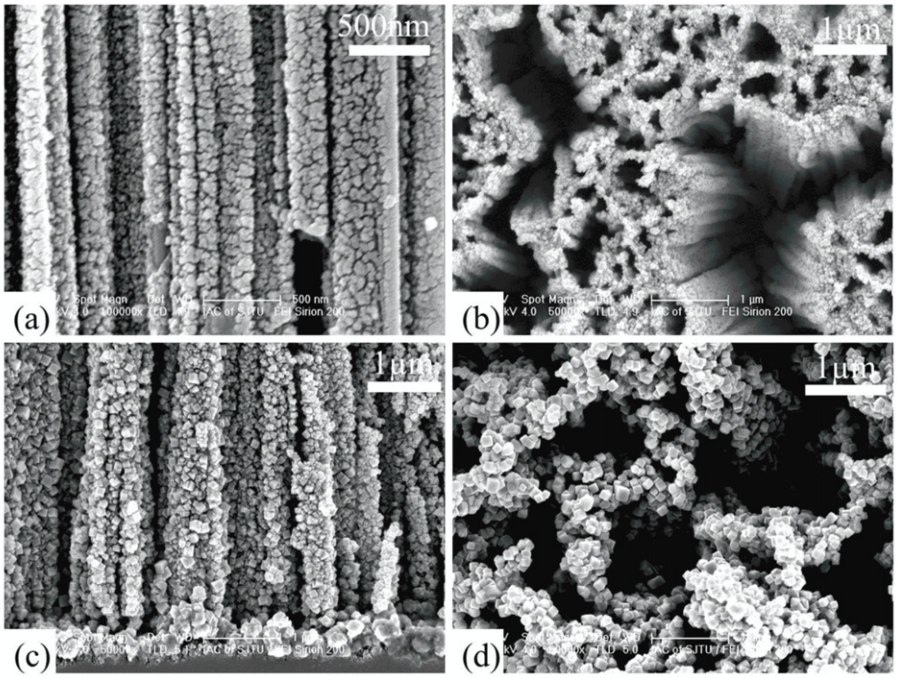

Figure 3. SEM images of Si NW/Cu_2O core–shell nanostructure: (a) cross-sectional view and (b) top-view of Si NW/Cu_2O core–shell nanostructure with 5 min deposition of Cu_2O nanocrystallite; (c) cross-sectional view and (d) top-view of Si NW/Cu_2O core–shell nanostructure with 15 min deposition of Cu_2O nanocrystallite.

Figure 4 shows TEM images of the Pt nanoparticles deposited on the surface of the Si NWs (figure 4(a)) and Si NW/Cu_2O core–shell structure (figures 4(b) and (c)). The size and the distribution of these Pt nanoparticles are not uniform, which can be seen clearly from the high-resolution TEM image of Pt nanoparticles on Cu_2O (figure 4(d)). When the deposition time was 10 min, the size of the biggest Pt nanoparticle was up to a dozen nanometers (figure 4(c)). In the high-resolution TEM image (figure 4(d)), the interplanar spacing of 0.22 nm corresponds to Pt(111), while 0.25 nm corresponds to Cu_2O(111).

The XRD pattern of the as-prepared core–shell nanosystem is shown in figure 5. The highest peak corresponds to the Si(400) phase from the Si NWs, which indicates

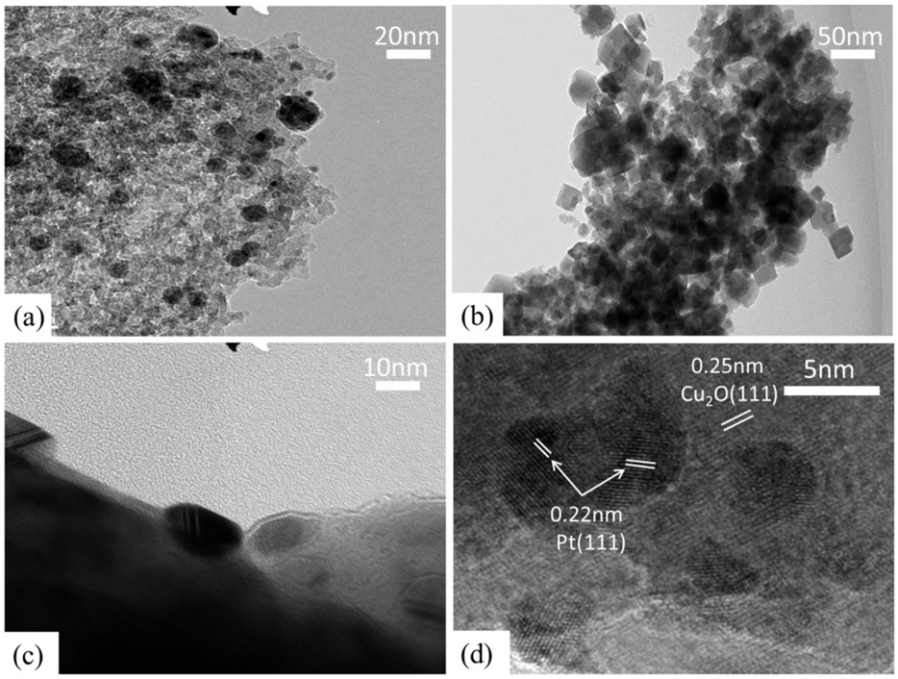

Figure 4. TEM images of Pt nanoparticles on Si NWs (a), Si NW/Cu_2O core–shell nanostructure (b) and (c), and high-resolution TEM of Pt nanoparticles on Cu_2O (d).

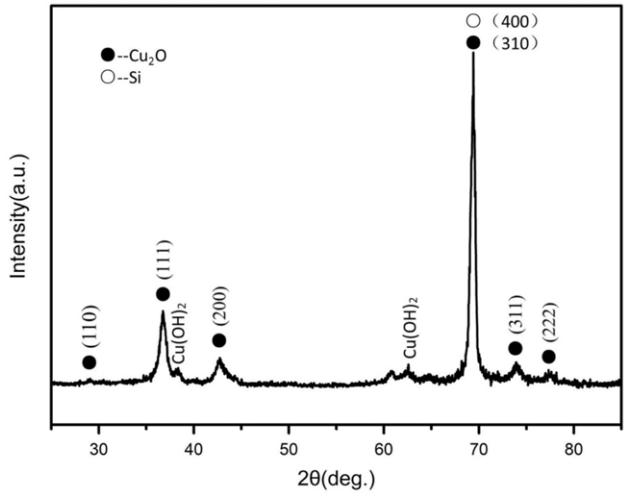

Figure 5. XRD pattern of the as-deposited Si NW/Cu_2O core–shell nanosystem.

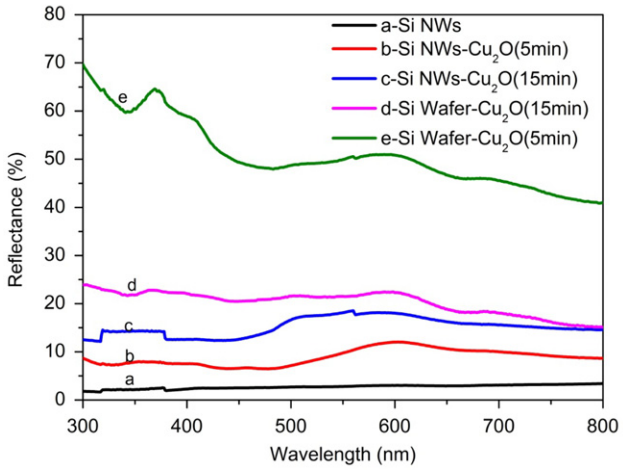

Figure 6. Reflectance spectra of Si NWs, planar Si/Cu_2O structure and Si NW/Cu_2O core–shell structure with different deposition times of Cu_2O nanocrystallite.

a strong orientation along the *c*-axis of the Si NWs. Besides the Si peak, several other peaks in the 2θ range of 25–85° are observed in the as-prepared Si NW/Cu_2O core–shell nanosystem, whose positions and relative intensity are found to identify the Cu_2O structure, which can be assigned to the (110), (111), (200), (310), (311) and (222) planes. In addition, there exist two tiny impurity peaks of $Cu(OH)_2$ in the sample.

Figure 6 shows the reflectance spectra of the as-prepared Si NWs, planar Si/Cu_2O and Si NW/Cu_2O core–shell nanosystem. The results indicated that the as-prepared Si NWs have excellent light absorption performance due to the array structure, porosity and the low energy gap of the material. For the Si NW/Cu_2O core–shell structure, the reflectivity would increase when the quantity of Cu_2O increased, which means that the light absorption performance would weaken to a certain extent. This could possibly be attributed to the vanishing of porosity and the slightly higher energy gap of the Cu_2O material. However, compared with a planar Si/Cu_2O structure, the Si NW/Cu_2O core–shell structure still has a lower reflectivity, that is, it has higher light absorption ability, which can be ascribed to light trapping effects of the NW array structure. For example, for a Si NW/Cu_2O structure

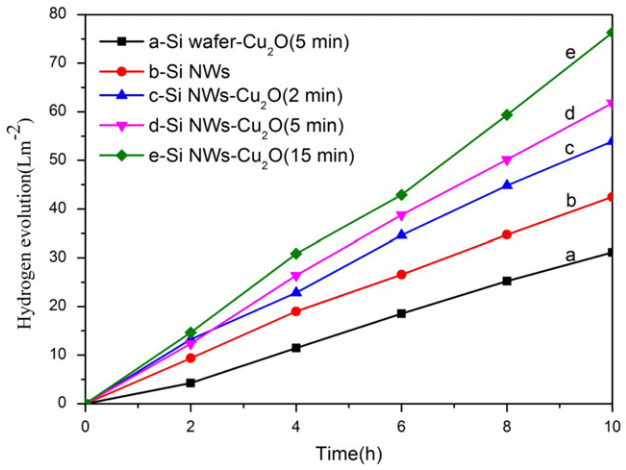

Figure 7. Photocatalytic H_2 evolution of Si NWs, planar Si/Cu_2O structure and Si NW/Cu_2O core–shell nanosystem under simulated sunlight irradiation.

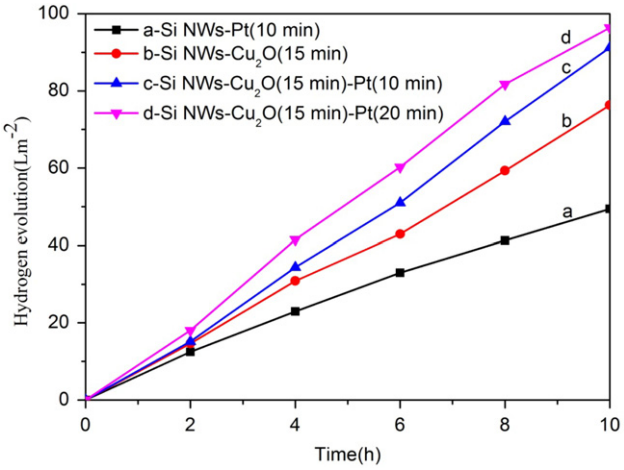

Figure 8. Photocatalytic H_2 evolution of Si NWs and Si NW/Cu_2O core–shell nanosystem with Pt nanoparticles as co-catalyst under simulated sunlight irradiation.

with 5 min deposition of Cu_2O, the reflectivity is only about 7–10%.

To study the photocatalytic activity of Si NW/Cu_2O nanocrystalline core–shell nanosystem further, the catalytic activity of Si NWs was first investigated. It is well known that single material Si alone offers relatively low H_2 evolution kinetics because of the competitive carrier recombination process. However, when a sacrificial agent exists, the carrier recombination process will be effectively restrained and the photocatalytic activity of Si NWs will be improved. The obtained Si NWs showed a certain photocatalytic hydrogen generation ability under visible-light irradiation (figure 7(b)). Comparing figures 7(c) and (b), we can see clearly that the Si NW/Cu_2O core–shell structure with 2 min deposition of Cu_2O has a better photocatalytic performance than that of the pure Si NWs in spite of a slightly lower light absorption performance than that of the Si NWs (they have almost the same surface area). This could be attributed to the formation of heterojunctions between p-type Cu_2O nanocrystallites and n-type Si NW arrays, which can accelerate the separation and transportation of photogenerated carriers effectively, thus minimizing carrier recombination. Besides, NW arrays further increase light absorption due to their excellent light trapping effects, which can be demonstrated by comparing figures 7(a) and (d). This is because a certain fraction of the reflected light would fall upon another area of the nanosystem in such a NW array structure and be available again for electron and hole generation instead of being lost to free space. Moreover, the photocatalytic performance of the core–shell nanosystem would be improved with the increase in the deposition time of Cu_2O nanocrystallites (from figures 7(c)–(e)). This is because the effective surface area of the core–shell nanosystem for photocatalytic reaction would be obviously augmented (figures 2(c) and 3(a) and (c)). Compared with Si NWs, the photocatalytic performance of a Si NW/Cu_2O core–shell nanosystem with 15 min deposition of Cu_2O increased nearly 50%.

In addition, as is well known that Pt is one of the most efficient co-catalysts in water splitting owing to its high work function and low Fermi energy. Moreover, metal Pt nanoparticles on the surface of the core–shell nanosystem would play certain role in protecting the composite structure catalyst, and then would improve the stability of it. In our experiments, we deposited Pt nanoparticles on the surface of Si NWs and a Si NW/Cu_2O core–shell nanosystem with 15 min deposition of Cu_2O to study their photocatalytic activity. The deposition times of Pt nanoparticles were 10 min and 20 min respectively. From figures 7(b) and 8(a)–(c), the photocatalytic activity of these nanosystems was enhanced observably after Pt loading. Furthermore, the Si NW/Cu_2O core–shell nanosystem with 10 min Pt deposition was superior to that of the Si NWs with 10 min Pt deposition. In addition, according to figures 8(c) and (d), the photocatalytic performance would be improved with the growing number and size increment of Pt nanoparticles. The hydrogen production ability of Si NW/Cu_2O (with 15 min deposition of Cu_2O) after 10 and 20 min Pt loading was about 30 and 45% better than that of a pure Si NW/Cu_2O nanosystem (with 15 min deposition of Cu_2O) (figures 8(b)–(d)).

4. Conclusions

We report a simple high-efficiency electroless deposition technique to construct a Si NW/Cu_2O core–shell heterojunction nanosystem photocatalyst for effective photocatalytic hydrogen generation from water splitting, where Cu_2O nanocrystallites were uniformly distributed on the surface of vertical Si NWs and formed heterojunctions with Si NWs. Even though the Si NW/Cu_2O core–shell structure has a slightly lower light absorption performance than that of the Si NWs, the photocatalytic performance of these core–shell nanosystems is still superior to pure Si NWs, due to a light trapping effect from the NW array structure and the formation of heterojunctions, thus improving charge separation and transportation, as well as the increased effective area for photoelectrochemical reaction from Cu_2O nanocrystallites. In

addition, the photocatalytic performance of Si NWs and the Si NW/Cu_2O nanocrystalline core–shell nanosystem would be improved observably after loading with a Pt nanoparticle co-catalyst, which can be attributed to the high work function and low Fermi energy of Pt nanoparticles.

Acknowledgments

This work was supported by National Major Basic Research Project of 2012CB934302, National 863 Program 2011AA050518, the Natural Science Foundation of China (grant nos 11174197 and 61234005), and Shanghai Jiao Tong University Innovation Fund for Postgraduates (no. Z-072-008).

References

[1] Fujishima A and Honda K 1972 Electrochemical photolysis of water at a semiconductor electrode *Nature* **238** 37–8
[2] Bolton J R, Strickler S J and Connolly J S 1985 Limiting and realizable efficiencies of solar photolysis of water *Nature* **316** 495–500
[3] Rajeshwar K 2007 Hydrogen generation at irradiated oxide semiconductor-solution interfaces *J. Appl. Electrochem.* **37** 765–87
[4] Ohtani B 2010 Photocatalysis A to Z-what we know and what we do not know in a scientific sense *J. Photochem. Photobiol.* C **11** 157–78
[5] Foley J M, Price M J, Feldblyum J I and Maldonado S 2012 Analysis of operation of the nanowire photoelectrodes for solar energy conversion *Energy Environ. Sci.* **5** 5203–20
[6] Maeda K and Domen K 2010 Photocatalytic water splitting-recent progress and future challenges *J. Phys. Chem. Lett.* **1** 2655–61
[7] Osterloh F E 2008 Inorganic materials as catalysts for photochemical splitting of water *Chem. Mater.* **20** 35–54
[8] Chen X B, Shen S H, Guo L J and Mao S S 2010 Semiconductor-based photocatalytic hydrogen generation *Chem. Rev.* **110** 6503–70
[9] Zhong M, Li Y B, Yamada I and Delaunay J J 2012 ZnO–$ZnGa_2O_4$ core–shell nanowire array for stable photoelectrochemical water splitting *Nanoscale* **4** 1509–14
[10] Reece S Y, Hamel J A, Sung K, Jarvi T D, Esswein A J, Pijpers J H, Nocera D G and Reece S Y 2011 Wireless solar water splitting using silicon-based semiconductors and earth-abundant catalysts *Science* **334** 645–8
[11] Bookbinder D C, Bruce J A, Dominey R N, Lewis N S and Wrighton M S 1980 Synthesis and characterization of a photosensitive interface for hydrogen generation-chemically modified p-type semiconducting silicon photocathodes *Proc. Natl Acad. Sci.* **77** 6280–4
[12] Bocarsly A B, Bookbinder D C, Dominey R N, Lewis N S and Wrighton M S 1980 Photoreduction at illuminated p-type semiconducting silicon photoelectrodes evidence for Fermi level pinning *J. Am. Chem. Soc.* **102** 3683–8
[13] Dominey R N, Lewis N S, Bruce J A, Bookbinder D C and Wrighton M S 1982 Improvement of photoelectrochemical hydrogen generation by surface modification of p-type silicon semiconductor photocathodes *J. Am. Chem. Soc.* **104** 467–82
[14] Nakato Y, Egi Y, Hiramoto M and Tsubomura H 1984 Hydrogen evolution and iodine reduction on an illuminated n–p junction silicon electrode and its application to efficient solar photoelectrolysis of hydrogen Iodide *J. Phys. Chem.* **88** 4218–22
[15] Kang Z H, Liu Y and Lee S T 2011 Small-sized silicon nanoparticles—new nanolights and nanocatalysts *Nanoscale* **3** 777–91
[16] Oh J, Deutsch T G, Yuan H C and Branz H M 2011 Nanoporous black silicon photocathode for H_2 production by photoelectrochemical water splitting *Energy Environ. Sci.* **4** 1690–4
[17] Wang F Y, Yang Q D, Xu G, Lei N Y, Tsang Y K, Wong N B and Ho J C 2011 Highly active and enhanced photocatalytic silicon nanowire arrays *Nanoscale* **3** 3269–76
[18] Zhang R Q, Liu X M, Wen Z and Jiang Q 2011 Prediction of silicon nanowires as photocatalysts for water splitting-band structures calculated using density functional theory *J. Phys. Chem.* C **115** 3425–8
[19] Oh I, Kye J and Hwang S 2011 Enhanced photoelectrochemical hydrogen production from silicon nanowire array photocathode *Nano Lett.* **12** 298–302
[20] Wang X, Peng K Q, Pan X J, Chen X, Yang Y, Li L, Meng X M, Zhang W J and Lee S T 2011 High-performance silicon nanowire array photoelectrochemical solar cells through surface passivation and modification *Angew. Chem. Int. Edn* **50** 9861–5
[21] Tian B, Zheng X L, Kempa T J, Fang Y, Yu N F, Yu G H, Huang J L and Lieber C M 2007 Coaxial silicon nanowires as solar cells and nanoelectronic power sources *Nature* **449** 885–90
[22] Hwang Y J, Boukai A and Yang P D 2009 High density *n*-Si-*n*-TiO_2 core–shell nanowire arrays with enhanced photoactivity *Nano Lett.* **9** 410–5
[23] Shi M M, Pan X W, Qiu W M, Zheng D X, Xu M S and Chen H Z 2011 Si-ZnO core–shell nanowire arrays for photoelectrochemical water splitting *Int. J. Hydrog. Energy* **36** 15153–9
[24] Fan G F, Zhu H W, Wang K L, Wei J Q, Li X M, Shu Q K, Guo N and Wu D H 2011 Graphene-silicon nanowire schottky junction for enhanced light harvesting *ACS Appl. Mater. Interfaces* **3** 721–5
[25] Sun K, Madsen K, Andersen P, Bao W N, Sun Z L and Wang D L 2012 Metal on metal oxide nanowire Co-catalyzed Si photocathode for solar water splitting *Nanotechnology* **23** 194013
[26] Baumeister P W 1961 Optical absorption of cuprous oxide *Phys. Rev.* **121** 359–62
[27] Nagasubramanian G, Gioda A S and Bard A J 1981 Photoelectrochemical behavior of p-type CuO in acetonitrile solutions *J. Electrochem. Soc.* **128** 2158–64
[28] Hara M, Kondo T, Komoda M, Ikeda S, Shinohara K, Tanaka A, Kondoa J N and Domen K 1998 Cu_2O as a photocatalyst for overall water splitting under visible light irradiation *Chem. Commun.* 357–8
[29] Xu L, Jiang L P and Zhu J J 2009 Sonochemical synthesis and photocatalysis of porous Cu_2O nanospheres with controllable structures *Nanotechnology* **20** 045605
[30] Paracchino1 A, Laporte V, Sivula K, Gratzel M and Thimsen E 2011 Highly active oxide photocathode for photoelectrochemical water reduction *Nature Mater.* **10** 456–61
[31] Hsu Y K, Yu C H, Chenb Y C and Linc Y G 2012 Hierarchical Cu_2O photocathodes with nano-microspheres for solar hydrogen generation *RSC Adv.* **2** 12455–9
[32] Zheng Z K, Huang B B, Wang Z Y, Guo M, Qin X Y, Zhang X Y, Wang P and Dai Y 2009 Crystal faces of Cu_2O and their stabilities in photocatalytic reactions *J. Phys. Chem.* C **113** 14448–53
[33] Barreca D, Fornasiero P, Gasparotto A, Gombac V, Maccato C, Montini T and Tondello E 2009 The potential of supported Cu_2O and CuO nanosystems in photocatalytic H_2 production *ChemSusChem* **2** 230–3

[34] Paracchino A, Mathews N, Hisatomi T, Stefik M, Tilley S D and Gratzel M 2012 Ultrathin films on copper(I) oxide water splitting photocathodes: a study on performance and stability *Energy Environ. Sci.* **5** 8673–81

[35] Paracchino A, Brauer J C, Moser J E, Thimsen E and Gratzel M 2012 Synthesis and characterization of high-photoactivity electrodeposited Cu_2O solar absorber by photoelectrochemistry and ultrafast spectroscopy *J. Phys. Chem.* C **116** 7341–50

[36] Hu C C, Nian J N and Teng H S 2008 Electrodeposited p-type Cu_2O as photocatalyst for H_2 evolution from water reduction in the presence of WO_3 *Sol. Energy Mater. Sol. Cells* **92** 1071–6

[37] Zhang S S, Zhang S Q, Peng F, Zhang H M, Liu H W and Zhao H J 2011 Electrodeposition of polyhedral Cu_2O on TiO_2 nanotube arrays for enhancing visible light photocatalytic performance *Electrochem. Commun.* **13** 861–4

[38] Tran P D, Batabyal S K, Pramana S S, Barber J, Wong L H and S C J Loo 2012 A cuprous oxide–reduced graphene oxide (Cu_2O–rGO) composite photocatalyst for hydrogen generation: employing rGO as an electron acceptor to enhance the photocatalytic activity and stability of Cu_2O *Nanoscale* **4** 3875–8

[39] Zhang Z H and Wang P 2012 Highly stable copper oxide composite as an effective photocathode for water splitting via a facile electrochemical synthesis strategy *J. Mater. Chem.* **22** 2456–64

[40] Wang Z H, Zhao S P, Zhu S Y, Sun Y L and Fang M 2011 Photocatalytic synthesis of M/Cu_2O (M = Ag, Au) heterogeneous nanocrystals and their photocatalytic properties *Cryst. Eng. Commun.* **13** 2262–7

[41] Li J T, Cushing S K, Bright J, Meng F K, Senty T R, Zheng P, Bristow A D and Wu N Q 2012 $Ag@Cu_2O$ core–shell nanoparticles as visible-light plasmonic photocatalysts *ACS Catal.* **3** 47–51

[42] Peng K Q, Hu J J, Yan Y J, Wu Y, Fang H, Xu Y, Lee S T and Zhu J 2006 Fabrication of single-crystalline silicon nanowires by scratching a silicon surface with catalytic metal particles *Adv. Funct. Mater.* **16** 387–94

[43] Peng K Q, Wu Y, Fang H, Zhong X Y, Xu Y and Zhu J 2005 Uniform, axial-orientation alignment of one-dimensional single-crystal silicon nanostructure arrays *Angew. Chem. Int. Edn* **44** 2737–42

[44] Sharma R and Hahn Y B 2012 Nanocrystalline thin films of Cu, CuO and Cu_2O synthesized by electroless deposition *Sci. Adv. Mater.* **4** 23–8